

Are Doppler Velocity Measurements Useful for Spinning Radar Odometry?

Daniil Lissus¹, Keenan Burnett¹, David J. Yoon¹, Richard Poulton², John Marshall², and Timothy D. Barfoot¹

Abstract—Spinning, frequency-modulated continuous-wave (FMCW) radars with 360° coverage have been gaining popularity for autonomous-vehicle navigation. However, unlike ‘fixed’ automotive radar, commercially available spinning radar systems typically do not produce radial velocities due to the lack of repeated measurements in the same direction and the fundamental hardware setup. To make these radial velocities observable, we modified the firmware of a commercial spinning radar to use triangular frequency modulation. In this paper, we develop a novel way to use this modulation to extract radial Doppler velocity measurements from single raw radar intensity scans without any required data association. We show that these noisy, error-prone measurements contain enough information to provide good ego-velocity estimates, and incorporate these estimates into different modern odometry pipelines. We extensively evaluate the pipelines on over 110 km of driving data in progressively more geometrically challenging autonomous-driving environments. We show that Doppler velocity measurements improve odometry in well-defined geometric conditions and enable it to continue functioning even in severely geometrically degenerate environments, such as long tunnels.

I. INTRODUCTION

Range-measuring sensors, such as radar and lidar, are now commonly used on autonomous vehicles (AVs) for tasks such as adaptive cruise control, crash warning systems, odometry, and localization. Lidar is generally more accurate than radar owing to its ability to capture returns from the full 3D environment at a high rate and accuracy [1]. Radar tends to have a longer range and is essentially unaffected by precipitation, fog, smoke, and sensor cleanliness. Radar has also traditionally been the only sensor capable of using the Doppler effect to estimate relative radial velocities of objects. As a result, there has been a recent increase in work attempting to leverage the unique advantages of radar [2].

AVs typically use frequency-modulated continuous-wave (FMCW) phased-array or spinning radars. Phased-array radars directly provide the range, elevation, radial cross section, and radial velocity of targets, but only operate on a limited field-of-view (FOV) [3]. In contrast, spinning radars provide a full 360° FOV, but typically only return the range and intensity of targets and not their relative velocities [4]. Spinning radars are preferred for navigation tasks such as odometry and localization, where a high degree of accuracy and awareness of all vehicles on the road is sought [5]. Using multiple phased-array radars for these tasks would require several sensors and extensive calibration. Additionally, most

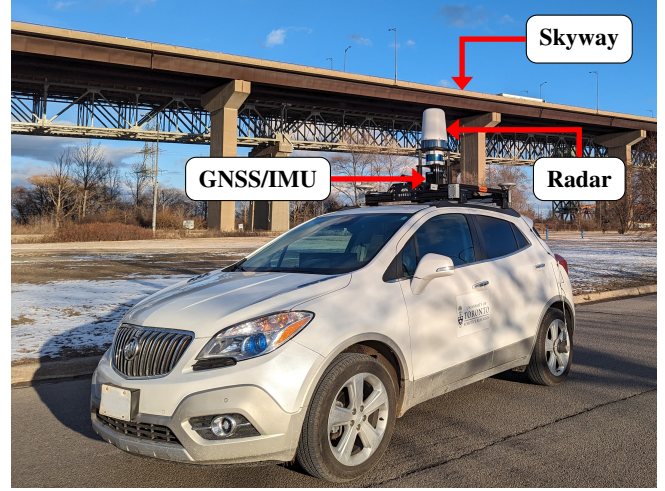


Fig. 1. Our data collection platform Boreas in front of the Burlington Bay James N. Allan Skyway, which has almost no on-road geometric features.

automotive phased-array radars directly provide extracted features instead of raw signal returns. This makes it harder to fine-tune the feature extraction process for specific tasks.

To expand the capabilities of spinning radar, we adopted a triangular frequency modulation scheme to allow extraction of Doppler velocity measurements. Our Doppler-enabled radar system, which we refer to as ‘spinning Doppler radar’, alternates its modulation pattern per azimuth, first increasing and then decreasing the frequency between consecutive azimuths. This makes it theoretically possible to extract the Doppler velocity of a target. However, in contrast to automotive radar, which provides accurate Doppler measurements from many repeated measurements of the same target [6], spinning radar typically has only a 50% overlap between consecutive azimuths. This means that a target is present in only two to three measurements per rotation at best. Thus, despite triangular modulation making it possible to extract Doppler velocities from spinning radar, it is unclear if they would be usable. This paper aims to answer the question: are Doppler measurements useful for spinning radar odometry?

Previously, Vivet *et al.* [7] used Doppler measurements for radar localization and mapping using a custom spinning Doppler radar. More recently, Rennie *et al.* [8] made use of the Doppler information from a Navtech RAS6 radar to train a neural network to directly predict vehicle pose information. However, they did not directly extract the Doppler velocity information, which makes it hard to evaluate its quality and impact. Additionally, both works halved the number of azimuths in order to extract Doppler information, and,

¹ University of Toronto Institute for Aerospace Studies (UTIAS), 4925 Dufferin St, Ontario, Canada. {daniil.lissus, keenan.burnett, david.yoon}@robotics.utias.utoronto.ca, tim.barfoot@utoronto.ca

² Navtech Radar, Home Farm, School Rd, Ardington, Wantage, Oxfordshire, UK. {richard.poulton, john.marshall}@navtechradar.com

in part because of this, do not produce results that are on par with modern state-of-the-art radar odometry approaches. We are thus revisiting the analytical approach presented by Vivet *et al.* [7] and refining it using modern approaches. As shown by Rennie *et al.* [8] and our own experiments, halving the resolution decreases performance of spinning radar odometry. We thus provide an approach to retain the full resolution while still extracting Doppler velocities. We evaluate our approach, and the usefulness of Doppler measurements, on a dataset collected in progressively more challenging environments ranging from a suburb to the geometrically degenerate skyway shown in Figure 1.

The main contributions of this paper are as follows:

- 1) We present a method to extract Doppler velocities using spinning radar, which modernizes and improves the prior work by Vivet *et al.* [7].
- 2) We demonstrate the use of these Doppler velocity measurements in different modern odometry pipelines.

The rest of the paper is organized as follows. Section II contextualizes the novelty claim. Section III discusses relevant radar theory and our Doppler velocity extraction approach. Section IV presents the dataset, evaluated pipelines, and experimental results. Finally, Section V concludes the paper and discusses future extensions.

II. RELATED WORK

A. Spinning Radar Navigation

Spinning radar navigation has recently seen a surge of interest [2], [9], [10]. Odometry and localization methods have typically been split into iterative closest point (ICP)-style pointcloud matching approaches [11]–[13], scan matching approaches [14], [15], and feature matching approaches [16], [17]. These have largely ignored Doppler-based distortion, and, owing to the limitations of previously available hardware, have not extracted Doppler measurements directly. Burnett *et al.* [18] corrected Doppler distortion in a spinning radar through the use of the vehicle ego-velocity estimate.

B. Automotive Doppler Radar

Kellner *et al.* [5] showed the ability of an automotive radar sensor to produce usable ego-motion estimates in combination with an Ackerman vehicle model. They did this by finding a least-squares fit to the measured point-wise radial Doppler velocities from points deemed stationary by Random Sample and Consensus (RANSAC) [19]. Additionally, they showed that the ego-motion estimation fails in the presence of many non-stationary targets, such as can be expected in heavy road traffic. This work was extended by Kellner *et al.* [20], where multiple radars were used in order to relax the requirement for a vehicle model; this is the first paper to show full 2D vehicle ego-motion estimation entirely using radar sensors. More recently, Galeote-Luque *et al.* [21] showed that Doppler measurements from an automotive radar can be used to do full 3D odometry by using RANSAC and a kinematic model. Instead of using RANSAC, Michaelis *et al.* [22] developed a dynamic object outlier rejection scheme using the previous ego-vehicle estimate. Gao *et al.* [3]

used Doppler measurements to undistort radar points in an uncertainty-aware way before using them in a probabilistic descriptor-based localization approach. Kubelka *et al.* [23] evaluated different automotive radar odometry pipelines and found that directly integrating high quality Doppler measurements with an IMU can outperform ICP-based methods in geometrically degenerate environments.

C. Spinning Doppler Radar

Two previous works have used Doppler measurements from spinning radar. Vivet *et al.* [7] developed a custom Doppler-enabled spinning radar and used it for the task of localization and mapping of a small mobile platform in simple outdoor environments. Our Doppler extraction approach is most similar to theirs, as both use cross-correlation. However, our extraction approach makes use of an additional filtering step, which we found crucial to achieve velocity estimates of high enough quality to be useful in an autonomous-driving context. Additionally, for a radar scan composed of N azimuths, our extractor produces $N - 1$ velocity estimates as compared to their $N/2$. Finally, their experiments were conducted in relatively slow (≤ 8.5 m/s) conditions without dynamic objects in the scene. We provide more extensive experimental results in multiple real autonomous-driving environments, with speeds reaching up to 28 m/s.

On the other hand, Rennie *et al.* [8] used a modern, commercially available Navtech RAS6 radar to estimate the vehicle ego-motion from the Doppler effect. This radar is functionally the same to the one that we use. However, their approach is entirely learning-based, as they feed their raw scans into a neural network to directly estimate the change in vehicle pose. They thus never directly extract Doppler measurements or estimate the ego-vehicle velocity explicitly. We propose a method to extract Doppler velocities, and show how they can be used in different ways to correct the ego-vehicle velocity, and, ultimately, position.

D. Doppler Lidar

It is also worth noting the development of FMCW lidar sensors, as they are also capable of providing Doppler measurements that have historically been unique to radar [24]. These sensors have thus far been limited to a fixed FOV, not unlike automotive radar. Doppler measurements from a commercially available FMCW lidar were shown to be effective at preventing ICP algorithm failure in degenerate geometric environments [25]. They were also shown to be useful in continuous-time odometry ICP [26] and at fast, correspondence-free velocity estimation [27]. We evaluate similar pipelines using a spinning radar in our experiments.

III. METHODOLOGY

A. Spinning Doppler Radar Theory

FMCW radar determines the range r to a target based on the difference between the received and transmitted signal frequencies Δf :

$$r = \frac{c \Delta f}{2S}, \quad (1)$$

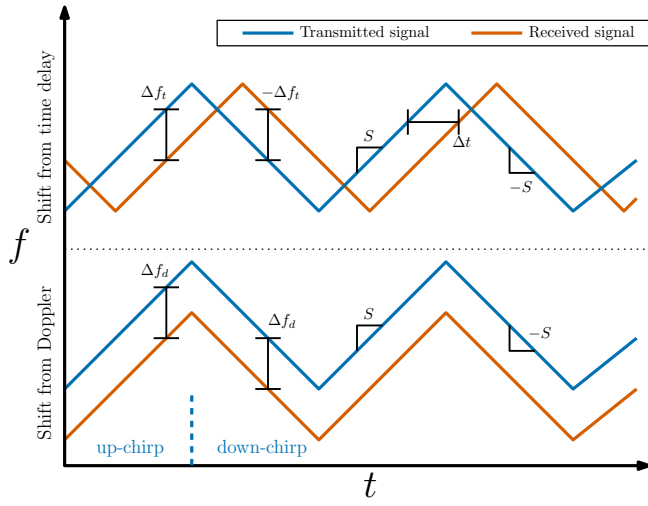


Fig. 2. A graphical representation of the shift in the frequency between the transmitted signal in blue and the received signal in orange for an FMCW radar with a triangular modulation pattern of slope S . The top shows a frequency shift Δf_t resulting from a time delay Δt induced by the signal traveling some distance. The bottom shows a frequency shift Δf_d resulting from the Doppler effect of an object moving away from the radar.

where c is the speed of light, S is the slope of the modulation pattern, and the division by 2 is present since the signal has to travel to and from the target. The difference in frequencies arises from two factors: the time delay Δt corresponding to the signal travelling to and from an object, and a Doppler-induced compression or expansion of the signal from the relative motion of a target. These two cases are visualized in Figure 2 for the case of a triangular modulation signal, where S is first positive ('up chirp') and then negative ('down chirp') in alternating fashion. When only a time-induced shift Δf_t is present, either chirp type produces the same range measurement (1), since the negatives in Δf and S cancel out for the down chirp. However, in the case of a Doppler-induced shift Δf_d , the range measurement will be impacted in opposite ways. This happens because the shift is constant for both chirps, whereas the slope of the modulation has a flipped sign. The opposite shift is shown in Figure 3, where azimuths in the lower image alternate between up and down chirp types creating a 'zig-zag' effect in what should be flat features. This is in contrast to the typically used sawtooth modulation pattern, which consists only of up chirps and thus has a constant Doppler shift. The opposite offset is what allows us to extract the Doppler velocity u , which is connected to Δf_d through the wavelength of the transmitted signal λ_t as

$$\Delta f_d = \frac{2u}{\lambda_t}. \quad (2)$$

The measured range from an up chirp with both shifts is

$$r_{\text{up}} = \frac{c\Delta f_t}{2S} + \frac{c\Delta f_d}{2S} = \tilde{r} + \Delta r_d, \quad (3)$$

where \tilde{r} is the true range to the target and Δr_d is the Doppler-induced range shift. For the down chirp, the range is

$$r_{\text{down}} = \frac{-c\Delta f_t}{-2S} + \frac{c\Delta f_d}{-2S} = \tilde{r} - \Delta r_d. \quad (4)$$

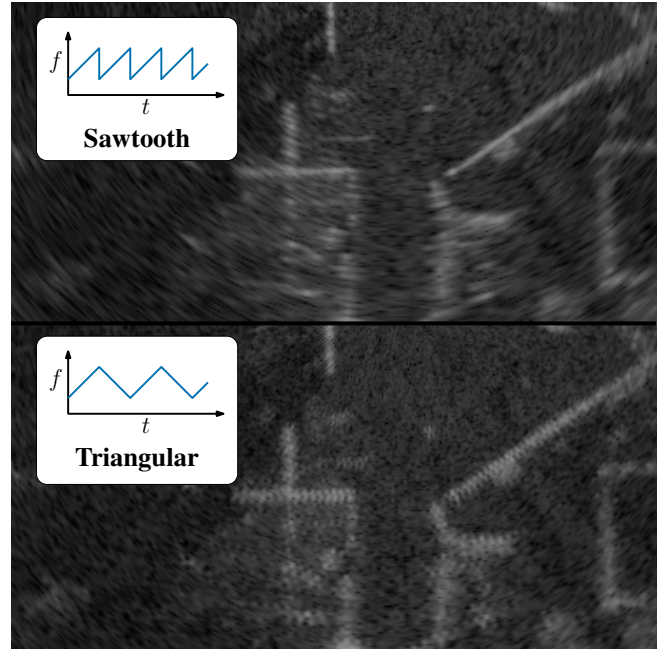


Fig. 3. Static features measured using a sawtooth (top) and triangular (bottom) modulated moving radar. The alternating Doppler-induced shift produced by the triangular signal modulation pattern can be seen as a 'zig-zag' in the intensity returns of continuous, flat features in the bottom image.

If a range measurement of the same target from both chirp types is recorded, we have a system of two equations and two unknowns. Solving this system for Δr_d , we can extract the corresponding relative velocity u , using $\beta = f_t/S$, as

$$\Delta r_d = \frac{c\Delta f_d}{2S} = \frac{2cu}{2\lambda_t S}, \quad (5a)$$

$$u = \frac{\Delta r_d S}{f_t} = \frac{\Delta r_d}{\beta}. \quad (5b)$$

B. Doppler Velocity Extraction

To extract the Doppler velocity measurement u for each point, we need to find the Doppler-induced range offset Δr_d for that point. This means obtaining range measurements from up and down chirp signals to use in (3) and (4). In our case, where azimuths alternate in chirp type, this would involve identifying points from consecutive azimuths that correspond to the same target. An alternative, entirely association-free way to find Δr_d is to instead consider the entire azimuth at once. If we assume that consecutive azimuths are looking at mostly the same targets, then consecutive return signals should be oppositely shifted by the same Δr_d . Thus, a cross-correlation between consecutive signals would yield a shift of $2\Delta r_d$. The downside of this is that only one velocity measurement is produced for each pair of azimuths. However, the measurement is then formed without needing to ever extract or match explicit points in the return signals. For radar systems that produces output as a continuous stream, such as the Navtech RAS6 radar, measurements can be formed at the same time as individual azimuths arrive.

The cross-correlation on the raw signals is very noisy and error-prone. Thus, a signal filtering step is first taken.

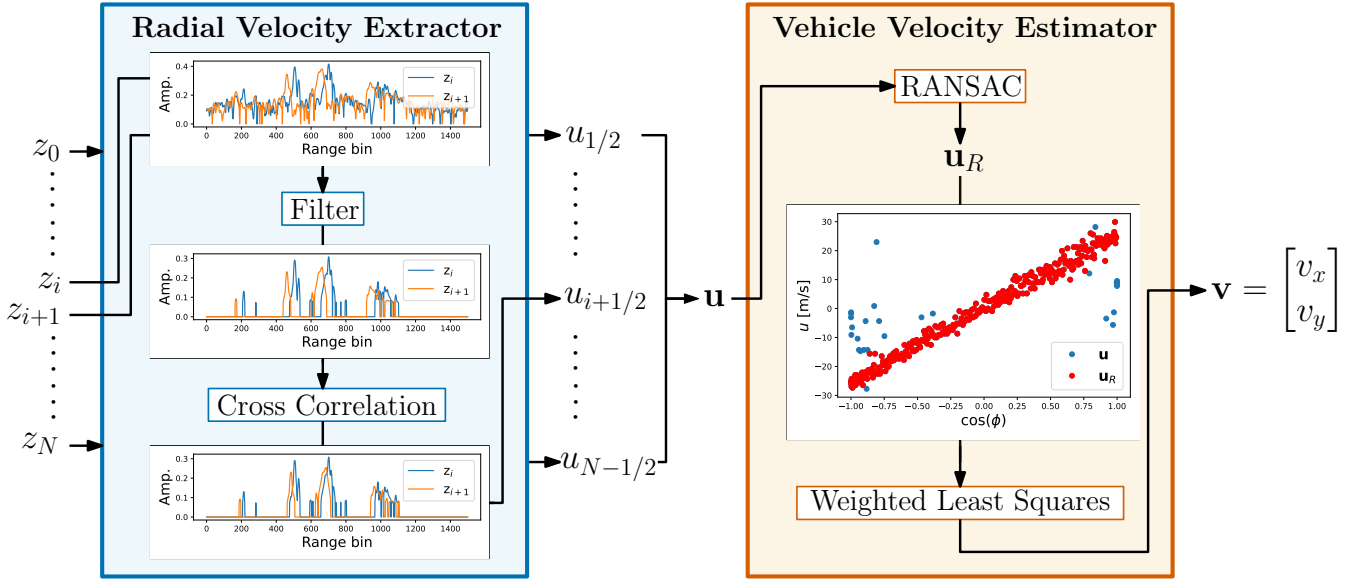


Fig. 4. The Doppler velocity estimation pipeline. First, raw radar intensity signals z_k , $k \in \{0, N\}$ for each azimuth ϕ are loaded into the radial velocity extractor. For each consecutive pair of azimuths, the extractor first filters the signals, and then runs a cross-correlation based on which a radial velocity u_j , $j \in \{1/2, N-1/2\}$ is computed. Radial velocities for the entire scan \mathbf{u} are passed through RANSAC to determine inliers, and then used in a weighted least squares algorithm with a Cauchy loss to estimate the ego-velocity \mathbf{v} .

We find that a modified version of the filtering approach previously applied to radar pointcloud extraction in [11] is highly effective in pre-processing the signals. Our filtering approach for each signal is as follows:

- 1) Subtract the mean.
- 2) Estimate the variance of the signal noise σ_s^2 (see [11]).
- 3) Apply a Gaussian filter ($\sigma_g = 15$).
- 4) Re-weight the smoothed signal by the probability that each bin does not correspond to noise (see [11]).
- 5) Zero out signal values less than $2.5\sigma_s$.

After filtering both azimuths, a normalized cross-correlation between the signals is performed to produce Δr_d and then u . The velocity is assigned to the in-between azimuth value of the two azimuths. As we compute one radial velocity measurement for each unique pair of N consecutive azimuths, we acquire $N-1$ measurements. This is in contrast to previous spinning Doppler radar works [7] and [8], which halved the number of used azimuths. This process is shown in the radial velocity extractor block of Figure 4.

C. Velocity Pseudo-Measurement Estimator

In general, the Doppler velocity extraction is prone to outliers and produces velocities with a relatively high distribution about the true value. To produce an ego-velocity pseudo-measurement, we combine all radial velocity measurements in an estimator. This is visualized in the vehicle velocity estimator block of Figure 4.

First, we run RANSAC with a relatively loose outlier rejection threshold (6 m/s) to filter out erroneous cross-correlation results and azimuths that correspond to dynamic objects. In environments where very few environmental points are present, it is easy for RANSAC to instead latch onto the dynamic objects in the scene. To overcome this

issue, we include a loose prior to the RANSAC model. This prior discards RANSAC candidate solutions that deviate too far, more than 6 m/s specifically, from the previous ego-velocity estimate, even if that candidate has a large number of inliers. We find that this is sufficient to mitigate the ‘capture’ of the velocity estimate by a large number of dynamic objects in the scene, without restricting our estimator. This is reminiscent of the approach taken in [22], although we make use of both the velocity from a previous timestep and RANSAC, whereas they forgo RANSAC.

After RANSAC, the inlier azimuth velocities are fed to a weighted least-squares (LS) algorithm. The LS algorithm estimates the forward v_x and side v_y ego-velocities as

$$\mathbf{v} = \begin{bmatrix} v_x \\ v_y \end{bmatrix}. \quad (6)$$

Given a vector of Doppler velocity measurements \mathbf{u} corresponding to azimuths ϕ , the algorithm iteratively minimizes the objective function $J(\mathbf{v})$:

$$J(\mathbf{v}) = \frac{1}{2} \mathbf{e}(\mathbf{v})^T \mathbf{W} \mathbf{e}(\mathbf{v}), \quad (7)$$

$$\mathbf{e}(\mathbf{v}) = [\cos \phi \quad \sin \phi] \mathbf{v} - \mathbf{u}, \quad (8)$$

$$\mathbf{W} = \text{diag} \left(\frac{1}{1 + (\mathbf{e}(\mathbf{v})/\rho)^2} \right), \quad (9)$$

where the cosine and sine operators act element-wise on ϕ and \mathbf{W} corresponds to a Cauchy weight with parameter ρ , which we set to 0.8. Finally, it was found that a velocity-dependent bias existed in the ego-velocity estimates. A linear model was fit to holdout data and used to subtract off the bias during experiments.

This approach generates a single ego-velocity estimate per radar scan, to which we assign a timestamp corresponding to

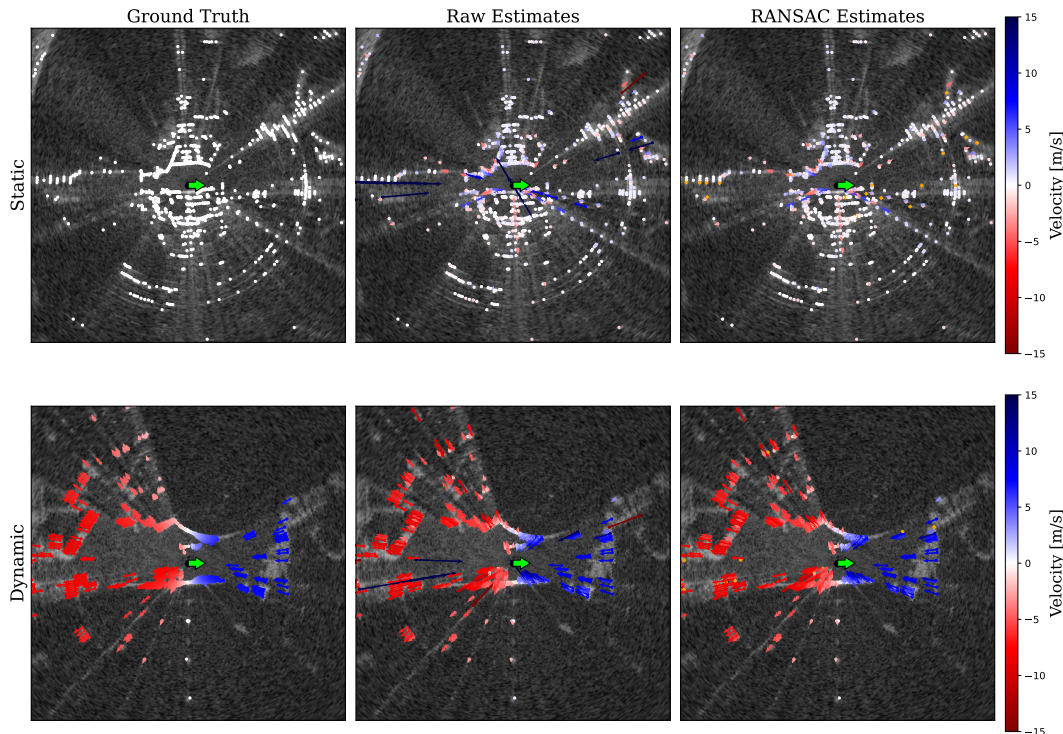


Fig. 5. Groundtruth and estimated radial velocities projected onto a pointcloud extracted from a raw radar scan in a static and dynamic scene. Velocities shown in the raw estimates column correspond to the initial association-free Doppler velocity estimation. Velocities shown in the RANSAC estimates column correspond to RANSAC-processed velocities, with rejected velocities coloured in orange. The vehicle orientation is shown as a green arrow.

the middle of the scan. In the future, we hope to implement a continuous-time estimator to properly account for the timestamp at which each Doppler velocity is received. Since most radars return only a few hundred azimuths per 360° sweep (400 for the Navtech RAS6 radar), this estimation is extremely fast. Although we find that using a Cauchy loss is necessary for best performance, it may be sufficient to use an unweighted LS algorithm depending on the requirements of the application. In this case, the estimation problem becomes linear in \mathbf{v} and can be solved in one step.

Figure 5 shows a qualitative result of the pipeline. In the figure, estimated azimuths are projected onto points extracted using the BFAR extractor [28] for visual clarity. The groundtruth radial velocities are generated by projecting the groundtruth vehicle ego-velocity onto each azimuth. It can be seen that the raw extracted radial velocities have obvious outliers, which are removed using RANSAC.

IV. EXPERIMENTS

A. Considered Pipelines

1) *Radar ICP Baselines*: The two baseline pipelines are based on the Teach and Repeat localization framework [29] used in [12]. Radar scans are used to extract pointclouds, which are then fed to ICP to produce an odometry estimate. The $SE(2)$ pose and $\boldsymbol{\varpi} = [v_x \ v_y \ \omega]^T$ ego-velocity is estimated in continuous time. The ego-velocity estimate is used to compensate for the Doppler-based range offset in the pointclouds. Please refer to [12] for full details. The only

difference between the baselines (‘B1’ and ‘B2’ in Table I) is that ‘B2’ additionally adds in a preintegrated heading gyroscope factor between consecutive radar frames. These pipelines are relatively slow due to ICP.

2) *Doppler Radar ICP*: Two new spinning radar odometry pipelines directly extend the baselines. These pipelines (‘N1’ and ‘N2’ in Table I) add a Doppler measurement-based term to the optimization problem. As discussed in Section III-C, the Doppler measurement estimator is used to estimate a forward and side ego-velocity \mathbf{v} for the timestamp at the midpoint of each scan. This estimate is then included as an additional cost term in the radar ICP pipelines by querying the continuous-velocity estimate at the scan midpoint timestamp and contrasting it with \mathbf{v} . A fixed noise covariance is tuned for this loss term. The added term is used both without (N1) and with (N2) a preintegrated heading gyroscope factor. These pipelines are relatively slow due to ICP.

3) *Doppler Radar + Gyroscope*: The final novel spinning radar odometry pipeline (‘N3’ in Table I) is adapted from [27] and directly integrates Doppler-based linear velocity pseudo-measurements \mathbf{v} and preintegrated heading gyroscope factors to estimate a pose. This is done by taking one Doppler-based pseudo-measurement and one preintegrated gyroscope factor per radar scan and integrating them forward by the timestep needed to reach the next frame. This pipeline is extremely fast, but is highly dependent on the quality of the gyroscope. We do not estimate the gyroscope bias in any pipeline to allow a fair comparison with the N3 pipeline, where the bias is unobservable.

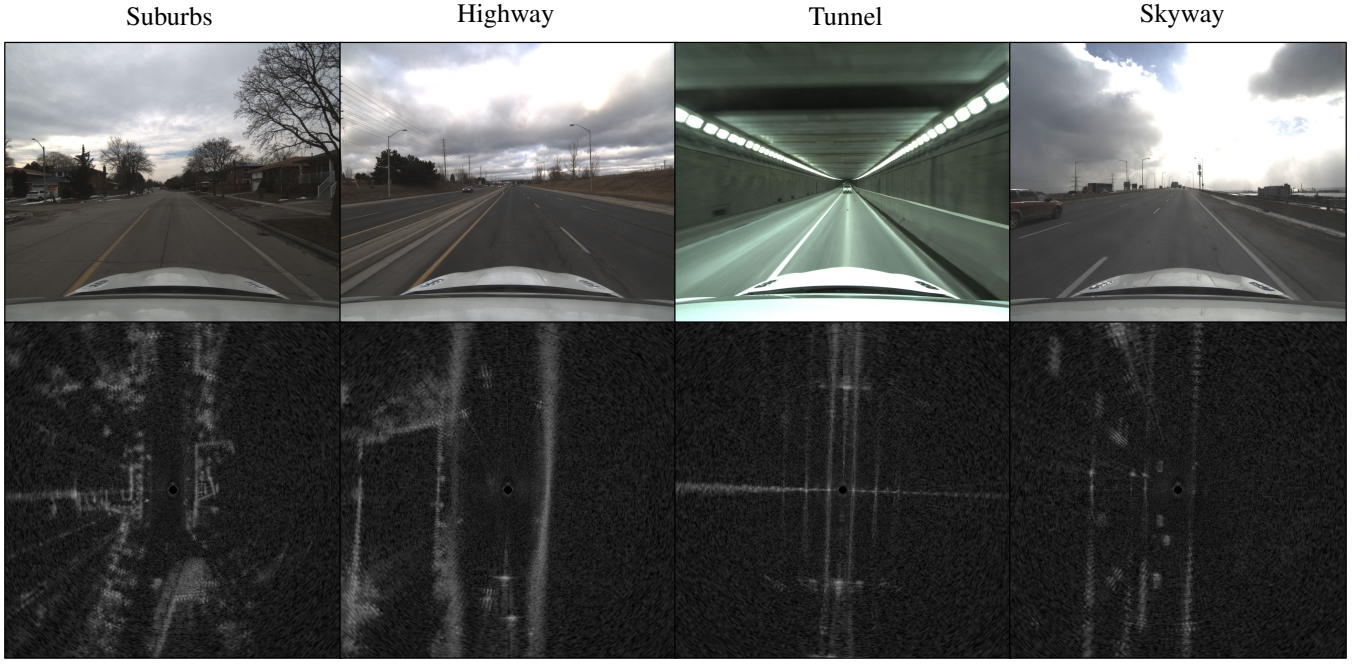


Fig. 6. A camera image and radar scan from each of the four trajectory types. The increase in difficulty for radar odometry from left to right can be observed in the fewer distinct geometric features.

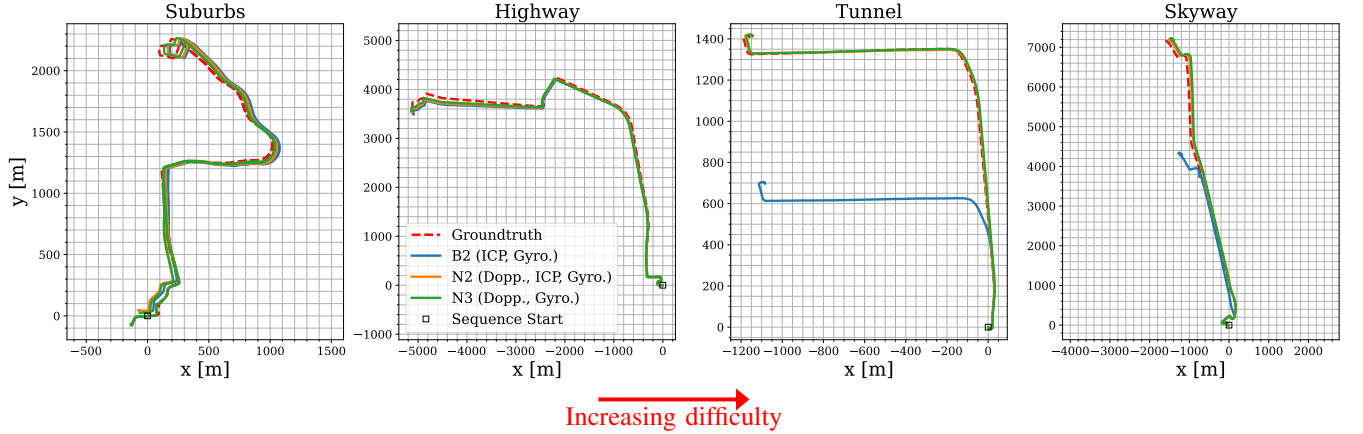


Fig. 7. Visualization of odometry performance for one sequence from each of the four types of trajectories. The baseline radar ICP with gyroscope data algorithm (B2) is shown alongside the two new algorithms (N2, N3) making use of spinning radar Doppler measurements. Groundtruth is shown as a red dotted line. The trajectories are presented in increasing order of difficulty from left to right. The new methods perform on par with the baseline in the two easiest cases, suburbs and highway, and continue to provide valid odometry results in the two harder cases, tunnel and skyway, where the baseline fails.

B. Dataset

We used the Boreas platform [4] to collect Doppler-enabled spinning radar data in progressively more challenging environments. Boreas is equipped with a Navtech RAS6 radar, which operates between 76 and 77 GHz, has a range resolution of 4.38 cm, spins at 4 Hz, and generates 400 azimuth measurements per rotation. The β parameter from (5a) is computed using the midpoint frequency of the ramp with a 0.944 correction factor applied to get the mean extracted velocity to better match the tuning data. The signal has a 3 dB beamwidth of 1.8° , meaning that consecutive azimuths overlap by 0.9° . This overlap lets us assume that consecutive signals have returns from the same targets. The groundtruth is generated from post-processed

GNSS, IMU, and wheel encoder data using Applanix’s RTX POSpac software. A caveat is that the gyroscope used for generating the groundtruth is the same one that is used in experiments, as it was the only gyroscope on the platform.¹ We use the unprocessed data in our algorithms, but it is nonetheless lightly correlated with the groundtruth.

We collected four repeated runs on four progressively more difficult sequences totaling approximately 111 km. Parameters were tuned on an additional 6 holdout sequences from a mix of sequence types. The sequence types are:

- 1) Suburbs (easy): These ≈ 7.9 km sequences follow the suburban Glen Shields route from [4] with speed limits

¹We plan to integrate a separate heading gyroscope in the future.

TABLE I
TRANSLATIONAL ODOMETRY DRIFT AND RUNTIME.

		Baselines		New		
		B1	B2	N1	N2	N3
	ICP	✓	✓	✓	✓	
	Gyro.		✓		✓	✓
	Dopp.			✓	✓	✓
Dopp. Extr.		~	~	45 ms	45 ms	45 ms
Odometry		136 ms	113 ms	110 ms	110 ms	1 ms
Total FPS		7.3	8.8	6.5	6.5	21.3
Suburbs	1	1.23%	0.59%	1.10%	0.58%	1.39%
	2	1.08%	0.58%	0.79%	0.44%	0.64%
	3	1.18%	0.54%	1.13%	0.51%	1.42%
	4	1.08%	0.42%	1.25%	0.42%	0.63%
	Avg.	1.14%	0.53%	1.07%	0.49%	1.02%
Highway	1	1.91%	0.91%	1.69%	0.67%	1.17%
	2	2.07%	0.62%	1.87%	0.57%	1.17%
	3	2.00%	0.63%	1.90%	0.50%	1.60%
	4	1.54%	0.44%	1.33%	0.40%	1.29%
	Avg.	1.88%	0.65%	1.70%	0.54%	1.31%
Tunnel	1	29.80%	29.43%	3.86%	0.56%	0.75%
	2	32.06%	31.75%	2.89%	0.45%	0.70%
	3	34.25%	33.83%	5.46%	0.71%	0.99%
	4	30.99%	29.82%	3.37%	0.49%	0.80%
	Avg.	31.77%	31.21%	3.90%	0.55%	0.81%
Skyway	1	36.58%	31.93%	4.05%	0.39%	0.64%
	2	3.14%	0.83%	2.44%	0.44%	0.64%
	3	58.17%	58.47%	7.14%	0.70%	0.73%
	4	56.77%	55.19%	5.58%	0.58%	0.76%
	Avg.	38.66%	36.60%	4.80%	0.53%	0.69%

of 30 – 60 km/h. All parts of the trajectory have multiple visible and unique geometric features.

- 2) Highway (medium): These ≈ 9.1 km sequences start in a suburban environment and then exit onto a highway with speed limits up to 80 km/h. Parts of the highway are geometrically challenging with only roadside barriers visible.
- 3) Tunnel (hard): These ≈ 2.5 km sequences drive through the 840 m long Thorold Tunnel in St. Catharines, Ontario, before turning onto a country road. The speed limit is up to 80 km/h. The inside of the tunnel is consistently geometrically degenerate, with only two continuous, parallel walls visible.
- 4) Skyway (hard): These ≈ 8.3 km sequences traverse the 2,560 m long Burlington Bay James N. Allan Skyway in Burlington, Ontario, with speed limits of up to 100 km/h. The skyway has large stretches with almost no visible static features, but many vehicles visible directly in front and behind the car. The static features that do exist are repetitive.

C. Odometry Results

The translational odometry drift from all pipelines is presented in Table I. The drift is reported as an average value of the KITTI-style odometry metrics [30] from subsequences of length (100, 200, ..., 800). We omit rotational drift

values for brevity and because they show similar trends. A visualization of the odometry is shown in Figure 7.

It can be seen that ICP-based methods generally drop in performance as the geometric difficulty of the sequences increases. For the two baselines, the estimation pipeline fails entirely as soon as the car enters the tunnel or skyway. All new pipelines that incorporate Doppler measurements produce functional odometry results regardless of the type of sequence. Using all available sources of information (N2) yields the best performance in all sequences and is the only ICP pipeline that maintains excellent performance ($\approx 0.5\%$ average drift) without dependence on the sequence type.

Despite losing out in performance to N2, directly integrating Doppler and gyroscope measurements (N3) performs well in all cases. This highlights the value that a heading gyroscope brings to an estimation pipeline, which we have similarly noted in our previous work [27], [31]. This is further supported by the root mean square error (RMSE) of the extracted Doppler velocities shown in Table II. Though the RMSE is lower in the suburbs and highway, direct integration performs the best in the tunnel and skyway, where there are few turns and the gyroscope is very reliable.

When gyroscope data is not used (B1 and N1), the extracted Doppler measurements noticeably improve results in 15 out of 16 sequences and prevent complete odometry failure in the tunnel and skyway. This result is achieved with only a slight computational costs needed to extract the measurements, but notably without any hardware changes.

Overall, our results draw parallels to the findings for automotive phased-array radar [23] and FMCW lidar [26]. Similarly to [26], we find that adding Doppler measurements to an ICP pipeline results in modest improvement in geometrically well-defined scenes and prevents failure in geometrically degenerate environments. When comparing to [23], we also find that directly integrating Doppler measurements with an inertial measurement sensor (IMU for them and heading gyroscope for us) performs remarkably well in all environments. However, they find that direct integration outperforms ICP-based methods in degenerate conditions, even when Doppler and IMU data is used as a prior. We find that using all available sources of information outperforms direct integration in all sequences. This difference may be due to [23] using an automotive phased-array radar with only an 80° FOV, which makes it more likely to only observe geometrically degenerate features as compared to a 360° spinning radar.

Table I also shows timing information based on single-thread performance of a Lenovo P1 Laptop with Intel(R) Core(TM) i7-12800H CPU @ 4.8 GHz and 32 GB of RAM. We list the Doppler extraction time, meaning the amount of time required to generate a Doppler pseudo-measurement according Figure 4, separately, as this can be theoretically run on the radar itself. The majority of this runtime comes from filtering each signal and computing a cross-correlation between neighbours, both of which could be done as azimuths arrive. All pipelines are real-time in the sense that they run faster than frames arrive (> 4 Hz).

TABLE II

EXTRACTED DOPPLER VELOCITY RMSE WITH MEAN IN BRACKETS.

	Suburbs	Highway	Tunnel	Skyway
x [m/s]	0.13 (0.01)	0.18 (0.02)	0.19 (-0.02)	0.18 (0.01)
y [m/s]	0.12 (0.01)	0.17 (0.00)	0.21 (-0.05)	0.27 (0.05)

V. CONCLUSION

This paper presents a method to analytically extract Doppler velocity measurements and makes use of them in modern radar odometry pipelines. We test our approach in four progressively more challenging environments: suburbs, highway, tunnel, and skyway. The use of Doppler measurements improves performance in easy geometric environments and maintains a useful level of performance in geometrically degenerate situations, where the baselines completely fail. We show this in both ICP-based pipelines and in a fast ego-velocity estimation pipeline, where odometry results are generated by directly integrating Doppler velocities and a gyroscope. In cases where a heading gyroscope is available and a fast solution is desired, the ego-velocity estimation pipeline is a promising solution. If best performance is desired or a gyroscope is not available, using our proposed Doppler measurement extraction improves results and prevents failures at no hardware cost while remaining real-time.

Future extensions to the work presented here will include evaluating the impact of Doppler measurements on mapping, localization, and object tracking.

ACKNOWLEDGMENT

This work was supported by the Ontario Graduate Scholarship (OGS) Program provided by the Province of Ontario.

REFERENCES

- [1] H. Yin, X. Xu, S. Lu, *et al.*, “A Survey on Global LiDAR Localization: Challenges, Advances and Open Problems,” *arXiv preprint arXiv:2302.07433*, 2023.
- [2] K. Harlow, H. Jang, T. D. Barfoot, A. Kim, and C. Heckman, “Survey on Recent mmWave Radar Applications in Robotics,” *arXiv preprint arXiv:2305.01135*, 2023.
- [3] P. Gao, S. Zhang, W. Wang, and C. X. Lu, “DC-Loc: Accurate Automotive Radar Based Metric Localization with Explicit Doppler Compensation,” in *2022 IEEE Int. Conf. Robot. Automat.*, 2022, pp. 4128–4134.
- [4] K. Burnett, D. J. Yoon, Y. Wu, *et al.*, “Boreas: A Multi-season Autonomous Driving Dataset,” *Int. J. Robot. Res. (IJRR)*, vol. 42, no. 1-2, pp. 33–42, 2023.
- [5] D. Kellner, M. Barjenbruch, J. Klappstein, J. Dickmann, and K. Dietmayer, “Instantaneous Ego-Motion Estimation Using Doppler Radar,” in *16th Int. IEEE Conf. Intell. Transp. Syst.*, IEEE, 2013, pp. 869–874.
- [6] V. Winkler, “Range Doppler Detection for Automotive FMCW Radars,” in *2007 Eur. Radar Conf.*, IEEE, 2007, pp. 166–169.
- [7] D. Vivet, P. Checchin, and R. Chapuis, “Localization and Mapping Using Only a Rotating FMCW Radar Sensor,” *Sensors*, vol. 13, no. 4, pp. 4527–4552, 2013.
- [8] F. Rennie, D. Williams, P. Newman, and D. De Martini, “Doppler-Aware Odometry from FMCW Scanning Radar,” in *26th Int. IEEE Conf. Intell. Transp. Syst.*, IEEE, 2023, pp. 5126–5132.
- [9] N. J. Abu-Alrub and N. A. Rawashdeh, “Radar Odometry for Autonomous Ground Vehicles: A Survey of Methods and Datasets,” *IEEE Trans. Intell. Vehicles*, 2023.
- [10] A. Venon, Y. Dupuis, P. Vasseur, and P. Merriaux, “Millimeter Wave FMCW Radars for Perception, Recognition and Localization in Automotive Applications: A Survey,” *IEEE Trans. Intell. Vehicles*, vol. 7, no. 3, pp. 533–555, 2022.
- [11] S. H. Cen and P. Newman, “Precise ego-motion estimation with millimeter-wave radar under diverse and challenging conditions,” in *2018 IEEE Int. Conf. Robot. Automat.*, IEEE, 2018, pp. 6045–6052.
- [12] K. Burnett, Y. Wu, D. J. Yoon, A. P. Schoellig, and T. D. Barfoot, “Are We Ready for Radar to Replace Lidar in All-weather Mapping and Localization?” *IEEE Robot. Automat. Lett.*, vol. 7, no. 4, pp. 10328–10335, 2022.
- [13] D. Adolfsson, M. Magnusson, A. Alhashimi, A. J. Lilienthal, and H. Andreasson, “Lidar-level Localization with Radar? The CFAR Approach to Accurate, Fast, and Robust Large-scale Radar Odometry in Diverse Environments,” *IEEE Trans. Robot.*, vol. 39, no. 2, pp. 1476–1495, 2022.
- [14] D. Barnes, R. Weston, and I. Posner, “Masking by Moving: Learning Distraction-Free Radar Odometry from Pose Information,” in *Conf. Robot Learn. (CoRL)*, 2019.
- [15] P. Checchin, F. Gérossier, C. Blanc, R. Chapuis, and L. Trassoudaine, “Radar Scan Matching SLAM Using the Fourier-Mellin Transform,” in *Field and Service Robot.: Results of the 7th Int. Conf.*, Springer, 2010, pp. 151–161.
- [16] D. Barnes and I. Posner, “Under the Radar: Learning to Predict Robust Keypoints for Odometry Estimation and Metric Localisation in Radar,” in *2020 IEEE Int. Conf. Robot. Automat.*, 2020.
- [17] K. Burnett, D. J. Yoon, A. P. Schoellig, and T. D. Barfoot, “Radar Odometry Combining Probabilistic Estimation and Unsupervised Feature Learning,” in *Robot.: Sci. and Syst.*, 2021.
- [18] K. Burnett, A. P. Schoellig, and T. D. Barfoot, “Do We Need to Compensate for Motion Distortion and Doppler Effects in Spinning Radar Navigation?” *IEEE Robot. Automat. Lett.*, vol. 6, no. 2, pp. 771–778, 2021.
- [19] M. A. Fischler and R. C. Bolles, “Random Sample Consensus: A Paradigm for Model Fitting With Applications to Image Analysis and Automated Cartography,” *Communications of the ACM*, vol. 24, no. 6, pp. 381–395, 1981.
- [20] D. Kellner, M. Barjenbruch, J. Klappstein, J. Dickmann, and K. Dietmayer, “Instantaneous Ego-motion Estimation Using Multiple Doppler Radars,” in *2014 IEEE Int. Conf. Robot. Automat.*, IEEE, 2014, pp. 1592–1597.
- [21] A. Galeote-Luque, V. Kubelka, M. Magnusson, J.-R. Ruiz-Sarmiento, and J. Gonzalez-Jimenez, “Doppler-only Single-scan 3D Vehicle Odometry,” *arXiv preprint arXiv:2310.04113*, 2023.
- [22] M. Michaelis, P. Berthold, T. Luettel, and H.-J. Wuensche, “Generating Odometry Measurements from Automotive Radar Doppler Measurements,” in *2023 IEEE Symp. Sensor Data Fusion Int. Conf. Multisensor Fusion Integration (SDF-MFI)*, IEEE, 2023, pp. 1–8.
- [23] V. Kubelka, E. Fritz, and M. Magnusson, “Do we need scan-matching in radar odometry?” *arXiv preprint arXiv:2310.18117*, 2023.
- [24] D. Pierrotet, F. Amzajerjian, L. Petway, B. Barnes, G. Lockard, and M. Rubio, “Linear FMCW Laser Radar for Precision Range and Vector Velocity Measurements,” *MRS Online Proceedings Library (OPL)*, vol. 1076, 1076–K04, 2008.
- [25] B. Hexsel, H. Vhavle, and Y. Chen, “DICP: Doppler Iterative Closest Point Algorithm,” in *Rob.: Sci. and Syst.*, New York City, NY, USA, 2022.
- [26] Y. Wu, D. J. Yoon, K. Burnett, *et al.*, “Picking Up Speed: Continuous-Time Lidar-Only Odometry using Doppler Velocity Measurements,” *IEEE Robot. Automat. Lett.*, vol. 8, no. 1, pp. 264–271, 2022.
- [27] D. J. Yoon, K. Burnett, J. Laconte, *et al.*, “Need for Speed: Fast Correspondence-Free Lidar-Inertial Odometry Using Doppler Velocity,” in *2023 IEEE/RSJ Int. Conf. Intell. Robot. Syst.*, IEEE, 2023, pp. 5304–5310.
- [28] A. Alhashimi, D. Adolfsson, M. Magnusson, H. Andreasson, and A. J. Lilienthal, “BFAR-bounded False Alarm Rate Detector for Improved Radar Odometry Estimation,” *arXiv preprint arXiv:2109.09669*, 2021.
- [29] P. Furgale and T. D. Barfoot, “Visual Teach and Repeat for Long-range Rover Autonomy,” *J. Field Rob.*, vol. 27, no. 5, pp. 534–560, 2010.
- [30] A. Geiger, P. Lenz, C. Stiller, and R. Urtasun, “Vision Meets Robotics: The KITTI Dataset,” *Int. J. Rob. Res.*, vol. 32, no. 11, pp. 1231–1237, 2013.
- [31] K. Burnett, A. P. Schoellig, and T. D. Barfoot, “Continuous-Time Radar-Inertial and Lidar-Inertial Odometry using a Gaussian Process Motion Prior,” *arXiv preprint arXiv:2402.06174*, 2024.